

Cite this: *RSC Adv.*, 2019, 9, 13201

Simultaneous size manipulation and red upconversion luminescence enhancement of $\text{CaF}_2\text{:Yb}^{3+}/\text{Ho}^{3+}$ nanoparticles by doping with Ce^{3+} ions

Xu Yang,^{ac} Maohui Yuan,^{ac} Rui Wang,^{ac} Xiaofan Zhao,^{ac} Zining Yang,^{ac} Kai Han,^{bc} Hongyan Wang^{ac} and Xiaojun Xu^{abc}

Harnessing the color tuning capability of upconversion nanoparticles (UCNPs) is of great significance in the field of advanced bioimaging and color display. Here, we report the tunable size and upconversion luminescence (UCL) multicolor in $\text{CaF}_2\text{:Yb}^{3+}/\text{Ho}^{3+}/\text{Ce}^{3+}$ UCNPs, which were synthesized by a facile hydrothermal method. It was found that the size of these UCNPs could be controlled (from 600 to 30 nm) by varying the concentration of Ce^{3+} ions. Under the excitation of a 980 nm continuous-wave (CW) laser, the UCL color of these UCNPs can be tuned from green to red as the doped Ce^{3+} ions gradually increase from 0 to 10 mol% and the red-to-green (R/G) ratio is enhanced remarkably. It is suggested that the cross-relaxation (CR) processes between Ho^{3+} and Ce^{3+} ions contribute to the tunable multicolor and enhancement of the R/G ratio. The mechanism of these processes is well supported by the time-resolved decay and near infrared (NIR) emission measurements.

Received 23rd March 2019

Accepted 23rd April 2019

DOI: 10.1039/c9ra02232e

rsc.li/rsc-advances

1. Introduction

UCNPs doped with lanthanide ions are a unique category of luminescent materials featuring abundant electronic transition in 4f electron shells, possessing remarkable optical properties, such as a sharp emission peak, long luminescence decay time and extremely low susceptibility to the chemical environment. These materials have the capability to upconvert two or more low energy photons into one high energy photon, with various emission bands ranging from violet to infrared.^{1–3} Over the past decade, this anti-Stokes optical property has advanced a broad range of applications, including bioimaging,^{4,5} lasers,⁶ anti-counterfeiting,⁷ photovoltaics,^{8,9} drug delivery,^{10,11} and solar energy harvesting.¹² In particular, manipulating the upconversion (UC) color of UCNPs has gained tremendous attention throughout the past few years due to its promise for applications in multiplex biological labelling,^{13,14} color display,^{15,16} and imaging.^{17,18} Moreover, owing to being located in the “optical window” of bio-tissues and cells, red UC emission centered at 650 nm is favored by application in the biomedicine area.^{19,20} In addition, when the luminescence color is tuned from green to

red (even a single-red-band), it presents much better chromatic purity, resulting in a much higher spatial resolution in biomedical field applications (*e.g.* bioimaging).^{11,21} Thus, it is of great significance to achieve enhancing red UCL in lanthanide doped nanoparticles through color manipulation.

Up to now, effective and controllable approaches have been implemented to tune the UCL color, including controlling the power density of excitation laser,²² varying the excitation pulse width and wavelength,^{23,24} changing temperature,²⁵ modulating the doping concentration and introducing suitable doping ions.^{26–29} However, except the last two methods, most of them could be hindered by extra requirements for laser sources and experimental environment in specific applications. So far, many UC materials have easily realized red emission, for example, $\text{NaYF}_4\text{:Yb}^{3+}/\text{Er}^{3+}$ nanoparticles facilitating red UC emission by increasing the concentration of Yb^{3+} ions, $\text{NaYF}_4\text{:Yb}^{3+}/\text{Er}^{3+}$ ($\text{Yb}^{3+}/\text{Ho}^{3+}$) nanoparticles emitting red UC emission *via* codoping with Mn^{2+} , Fe^{3+} or Pb^{2+} .^{11,18,30,31}

$\text{Yb}^{3+}/\text{Ho}^{3+}$ codoped UCNPs are one of the most efficient UC materials and have been widely studied. Generally, under the excitation of 980 nm CW laser, $\text{Yb}^{3+}/\text{Ho}^{3+}$ codoped UCNPs mainly exhibit green (${}^5\text{S}_2/{}^5\text{F}_4 \rightarrow {}^5\text{I}_8$, 540 nm) and red (${}^5\text{F}_5 \rightarrow {}^5\text{I}_8$, 650 nm) UC emissions. It should be mentioned that the red UC emission closely associated with two extra non-radiative relaxation (NR) processes (${}^5\text{I}_6 \rightarrow {}^5\text{I}_7$ and ${}^5\text{S}_2/{}^5\text{F}_4 \rightarrow {}^5\text{F}_5$). Consequently, altering these two NR processes could effectively change the red UC emission radiative probability and modulate the luminescence color. Based on the analysis above, Zhang

^aCollege of Advanced Interdisciplinary Studies, National University of Defence Technology, Changsha, 410073, China. E-mail: yuanmaohuino1@126.com; wanghongyan@nudt.edu.cn

^bState Key Laboratory of Pulsed Power Laser Technology, National University of Defence Technology, Changsha, 410073, China

^cHunan Provincial Key Laboratory of High Energy Laser Technology, National University of Defence Technology, Changsha, 410073, China



et al. reported the single-red-band UC emission in $\text{NaYF}_4:\text{Yb}^{3+}/\text{Ho}^{3+}$ nanoparticles by codoping with Ce^{3+} ions for the first time.³² Moreover, similar phenomenon has been demonstrated in NaGdF_4 , NaLuF_4 , LiYbF_4 , $\text{AgLa}(\text{MoO}_4)_2$ and Sr_2GdF_7 host lattices.^{33–37} Actually, CaF_2 is also an important yet understudied UCNP due to its low phonon energy, easy substitution by lanthanide ions and non-toxicity to biological tissues, which has been widely applied in biological fields such as biological labelling^{38,39} and drug delivery.⁴⁰ Besides, the Ce^{3+} ion has a larger ionic radius than Ca^{2+} ion. This indicates that the incorporation of Ce^{3+} ions in $\text{CaF}_2:\text{Yb}^{3+}/\text{Ho}^{3+}$ UCNP would vary the particle size of the CaF_2 host lattice. The simultaneous size manipulation and UCL multicolor tunability, especially dominant red emission of UCNP could meet the growing demand in biological applications. However, relevant studies are still challenging and rarely reported. Until now, this has been realized in $\text{Yb}^{3+}/\text{Er}^{3+}$ codoped UCNP by doping with Fe^{3+} and Mn^{2+} ions.^{18,41} To the best of our knowledge, Ce^{3+} -induced UCL multicolor and size manipulation of $\text{Yb}^{3+}/\text{Ho}^{3+}$ codoped UCNP has never been reported so far.

In this work, we synthesized the Ce^{3+} doped $\text{CaF}_2:\text{Yb}^{3+}/\text{Ho}^{3+}$ UCNP through a hydrothermal method. The influence of Ce^{3+} concentration on the size and phase of CaF_2 nanoparticles was studied in detail. Under the excitation of 980 nm CW laser, the UCL color of these UCNP can be tuned from green to red as the doped Ce^{3+} ions increase from 0 to 10 mol%. Moreover, the mechanism of the enhancement of red UC emission has been demonstrated by the measurements of fluorescence lifetime, NIR emission as well as the dependence of luminescence intensity on the excitation power.

2. Experimental details

2.1. Synthesis of $\text{CaF}_2:\text{Yb}^{3+}/\text{Ho}^{3+}/\text{Ce}^{3+}$ (20/2/*x* mol%) UCNP

The raw materials were purchased from Aladdin (China), including $\text{YbCl}_3 \cdot 6\text{H}_2\text{O}$ (99.9% metals basis), $\text{HoCl}_3 \cdot 6\text{H}_2\text{O}$ (99.9% metals basis), $\text{CeCl}_3 \cdot 7\text{H}_2\text{O}$ (99.9% metals basis), $\text{CaCl}_2 \cdot 2\text{H}_2\text{O}$ (99.99% metals basis), ethylenediaminetetraacetic acid (EDTA) (99% analytical grade) and NaBF_4 (99.99% metals basis). All the chemicals were used as received without further purification.

The $\text{CaF}_2:\text{Yb}^{3+}/\text{Ho}^{3+}/\text{Ce}^{3+}$ UCNP were synthesized by a modified hydrothermal procedure. The molar ratio of $(\text{Ln}^{3+} \& \text{Ca}^{2+})/\text{EDTA}/\text{NaBF}_4$ was fixed to 1 : 1 : 2. In a typical procedure, 2 mmol of chloride salts and 2 mmol EDTA were dissolved in 20 mL of deionized (DI) water and the mixtures were stirred vigorously for 1 h. Then, 20 mL of aqueous solution containing 4 mmol NaBF_4 was transferred to the aqueous solution prepared above. By stirring for another 1 h, a milky colloidal solution was obtained. Subsequently, the mixtures were transferred into a 50 mL Teflon-lined autoclave and heated at 200 °C for 30 h, and then slowly cooled down to room temperature. The precipitates were collected by centrifugation at 6000 rpm for 4 min, and washed with DI water and ethanol for several times, and dried at 40 °C for 12 h in air. Different dopant contents of UCNP were synthesized by varying the composition of the

RECl_3 and CaCl_2 while keeping the total RE^{3+} and Ca^{2+} ions constant at 2 mmol.

2.2. Physical characterization

The powder X-ray diffraction (XRD) patterns of the UCNP were measured by an X-ray diffractometer with Cu K α radiation at 40 kV and 200 mA (TTR III system, Rigaku), with the angular 2θ ranging from 20° to 80°. The scanning rate of the 2θ angle of the XRD spectra was 10° min⁻¹. Meanwhile, the size and morphology of these UCNP were characterized by transmission electron microscopy (TEM) (Tecnai G2 F20, FEI). Before the TEM test, all the samples were dispersed in ethanol and sonicated for 10 min, and a drop of the solution of each sample was evaporated on a copper mesh grid supported by a carbon film.

2.3. Photoluminescence measurements

The UCNP were dispersed in ethanol and irradiated by 980 nm CW laser with a focus diameter of 4 mm. The UCL was collected by a lens coupled grating monochromator (Omni- λ 3072i, Zolix) with an integrated photomultiplier tube (PMT-H-S1-R928). For the NIR emission measurements, a NIR spectrometer (NIR 1700, ideaoptics) was utilized. The decay profiles of UC emissions were recorded by a digital oscilloscope (1 GHz, InfiniiVision DSOX6002A, KEYSIGHT) and a nanosecond pulsed 980 nm laser used as the excitation source (the repetition rate is 10 Hz and the pulse duration is 20 ns). All the above experiments were carried out at room temperature.

3. Results and discussion

The morphology and phase of the as-prepared $\text{CaF}_2:\text{Yb}^{3+}/\text{Ho}^{3+}/\text{Ce}^{3+}$ UCNP were characterized by TEM and XRD. Fig. 1(a–f) present the TEM micrographs of the $\text{CaF}_2:\text{Yb}^{3+}/\text{Ho}^{3+}$ (20/2 mol%) UCNP doped with 0, 2, 4, 6, 8 and 10 mol% Ce^{3+} ions, respectively. It could be seen that these UCNP are nearly monodispersed with uniform size distribution in each sample. The mean size of UCNP decreases from 600 to 30 nm with the doping Ce^{3+} ions increasing from 0 to 10 mol%. Notably, the size of the UCNP is independent on the doping Ce^{3+} ions (when

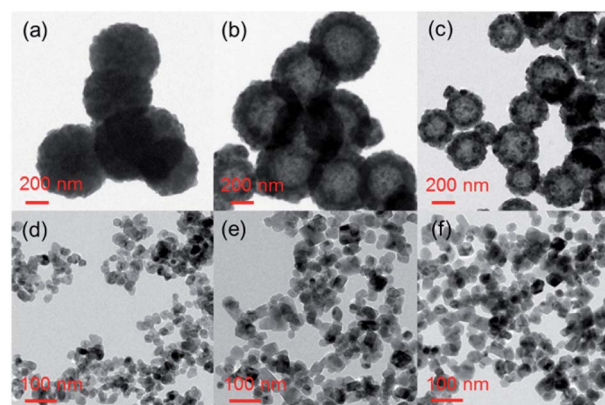


Fig. 1 (a–f) Typical TEM images of $\text{CaF}_2:\text{Yb}^{3+}/\text{Ho}^{3+}$ (20/2 mol%) UCNP doped with 0, 2, 4, 6, 8, 10 mol% Ce^{3+} ions, respectively.



the doping Ce^{3+} ions larger than 6 mol%), which always keep the approximate average size of 30 nm. The tunable size reduction of the UCNPs might attribute to the fact that the larger Ce^{3+} ions enter the CaF_2 host lattice by substituting relatively smaller Ca^{2+} ions.^{3,42}

Fig. 2 displays the XRD patterns of the $\text{CaF}_2:\text{Yb}^{3+}/\text{Ho}^{3+}$ UCNPs doping with different concentrations of Ce^{3+} ions. All the diffraction peaks match well with the standard peak positions of the cubic phase of CaF_2 materials (JCPDS no. 87-0976), which indicates that the as-prepared UCNPs are highly crystallized. It should be noted that the diffraction peaks shifted slightly towards lower angle, which is ascribed to the substitution of smaller Ca^{2+} ions by the relatively larger Ce^{3+} ions.

Fig. 3(a) illustrates the UC emission spectra of $\text{CaF}_2:\text{Yb}^{3+}/\text{Ho}^{3+}$ UCNPs doping with different Ce^{3+} ions (0, 4 and 10 mol%), and the insets exhibit the corresponding UCL color. Two typical UC emissions of Ho^{3+} ion can be observed under the excitation of 980 nm CW laser: green (541 nm) and red (650 nm) emission bands, attributing to the transitions of $^5\text{S}_2/^5\text{F}_4 \rightarrow ^5\text{I}_8$, and $^5\text{F}_5 \rightarrow ^5\text{I}_8$, respectively.

For Ce^{3+} -free UCNPs, it is found that the green emission (541 nm) is stronger than the red emission (650 nm), which exhibits a green luminescence color. By increasing the doping Ce^{3+} ions up to 4 mol%, the red emission is further enhanced, leading to the color changing from green to yellow. If the doping Ce^{3+} ions further increase to 10 mol%, the green UC emission is efficiently suppressed and the red UC emission is significantly enhanced, resulting in the luminescence color tuning from yellow to red. As presented in Fig. 3(b), we have calculated the CIE chromaticity coordinates of $\text{CaF}_2:\text{Yb}^{3+}/\text{Ho}^{3+}$ UCNPs doping with different concentrations of Ce^{3+} ions (0–10 mol%) based on their UCL spectra. The result reveals that a wide range of multicolor can be acquired by adjusting the concentrations of Ce^{3+} ions. This means that these UCNPs could be suitable for different applications.

To figure out the color tuning capability of $\text{CaF}_2:\text{Yb}^{3+}/\text{Ho}^{3+}/\text{Ce}^{3+}$ UCNPs in detail, UC samples with Ce^{3+} ions contents ranging from 0 to 10 mol% were prepared, and the corresponding UC spectra were measured as well. The R/G intensity ratio is calculated as exhibited in Fig. 4. When the Ce^{3+} concentration varies from 0 to 10 mol%, the R/G ratio can be promoted from 0.17 to 7.44. It indicates that the doping of Ce^{3+} ions plays an important role in tuning the luminescence color. To understand the mechanism of the UC emission, the population processes in $\text{CaF}_2:\text{Yb}^{3+}/\text{Ho}^{3+}/\text{Ce}^{3+}$ UCNPs are schematically demonstrated. As shown in Fig. 5(a), a proposed energy level diagram of Yb^{3+} , Ho^{3+} , Ce^{3+} ions and the relevant ET processes are also displayed. Under the excitation of 980 nm CW laser, the Yb^{3+} ions absorb the laser energy and the ground state ($^2\text{F}_{7/2}$) can be excited to the excited state ($^2\text{F}_{5/2}$). Next, Ho^{3+} ions are excited from ground state $^5\text{I}_8$ to $^5\text{I}_6$ through the efficient ET process between Yb^{3+} and Ho^{3+} ions, and a NR process occurs in the $^5\text{I}_6$ state, which leads to a population in the $^5\text{I}_7$ state. Similarly, $^5\text{F}_5$ and $^5\text{S}_2/^5\text{F}_4$ state of Ho^{3+} ions can be populated by the utilization the ET processes from the excited Yb^{3+} ions as well. Therefore, once these excited states are populated, the efficient UC emissions will generate, including the green ($^5\text{S}_2/^5\text{F}_4 \rightarrow ^5\text{I}_8$) and red ($^5\text{F}_5 \rightarrow ^5\text{I}_8$) emission, as well as a NIR ($^5\text{I}_6 \rightarrow ^5\text{I}_8$)

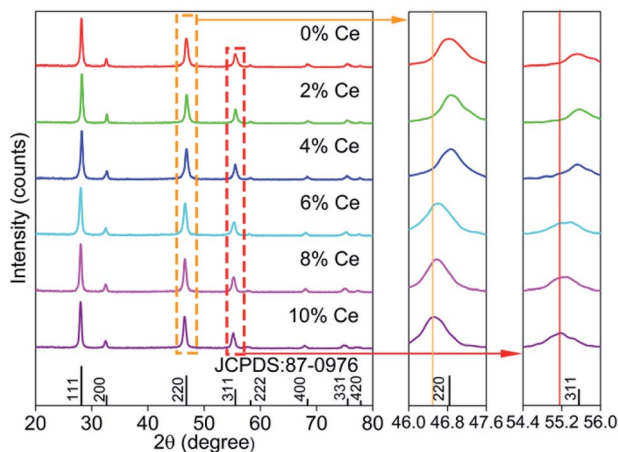


Fig. 2 XRD patterns of $\text{CaF}_2:\text{Yb}^{3+}/\text{Ho}^{3+}$ UCNPs doped with Ce^{3+} ions of 0–10 mol%, and its local magnification.

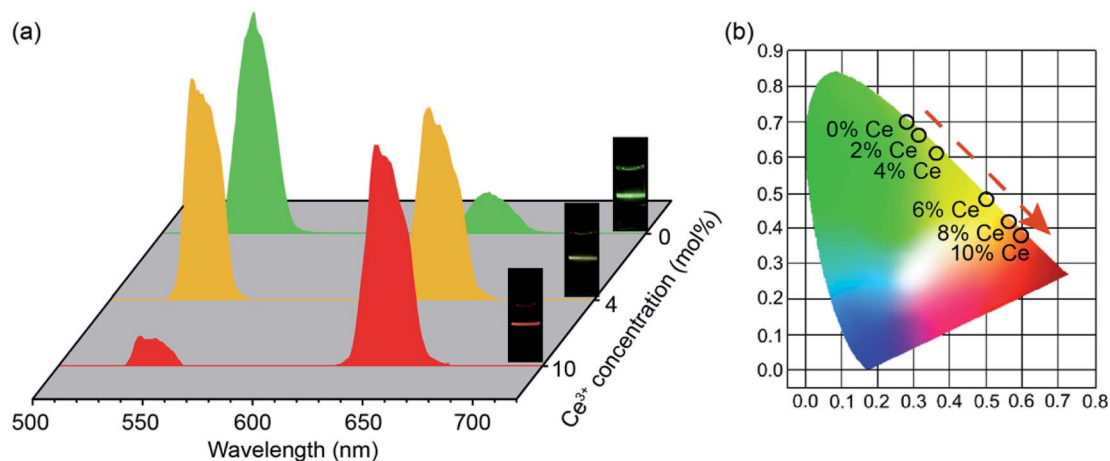


Fig. 3 (a) UC emission spectra of $\text{CaF}_2:\text{Yb}^{3+}/\text{Ho}^{3+}$ UCNPs doping with different concentrations of Ce^{3+} ions (0, 4 and 10 mol%) at the power density of 31.8 W cm^{-2} . The insets show the corresponding luminescence color of the UCNPs. (b) CIE chromaticity coordinates for the $\text{CaF}_2:\text{Yb}^{3+}/\text{Ho}^{3+}$ UCNPs doping with different concentrations of Ce^{3+} ions. All excitation wavelengths are at 980 nm.



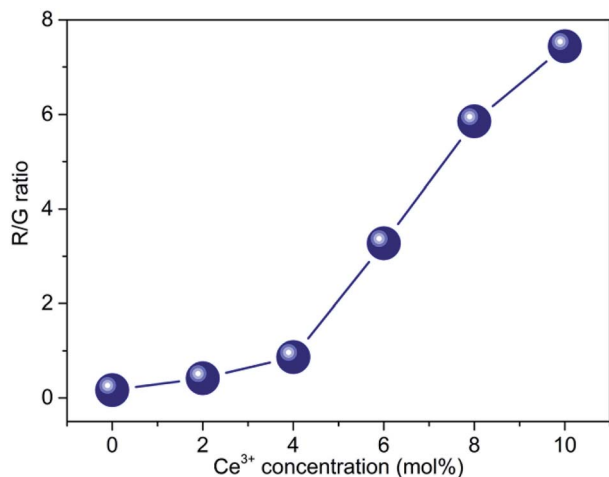


Fig. 4 The R/G ratio of $\text{CaF}_2:\text{Yb}^{3+}/\text{Ho}^{3+}$ UCNP s doped with different Ce^{3+} concentrations (0–10 mol%). (R and G represent red and green UC emissions, respectively.)

emission. It should be mentioned that the NR process from $^5\text{S}_2/^5\text{F}_4$ to the $^5\text{F}_5$ state also makes contribution to the red emission. As discussed in the section of introduction, the two NR processes ($^5\text{I}_6 \rightarrow ^5\text{I}_7$ and $^5\text{S}_2/^5\text{F}_4 \rightarrow ^5\text{F}_5$) could involve in the modulation of red emission of Ho^{3+} ions. It should be noted

that the phonon energy of CaF_2 host lattice ($\sim 350 \text{ cm}^{-1}$) is much lower than the energy gaps of $^5\text{S}_2/^5\text{F}_4 \rightarrow ^5\text{F}_5$ and $^5\text{I}_6 \rightarrow ^5\text{I}_7$ ($\sim 3000 \text{ cm}^{-1}$). This means that these two NR processes in CaF_2 UCNP s should occur inefficiently. However, the energy gap between the ground and excited states ($^2\text{F}_{5/2}$ and $^2\text{F}_{7/2}$) of Ce^{3+} ions is about 3000 cm^{-1} , which matches well with the value of energy gap of the above two NR processes. This results in a fact that these two NR processes are replaced by the following two CR processes: $^5\text{S}_2/^5\text{F}_4(\text{Ho}^{3+}) + ^2\text{F}_{5/2}(\text{Ce}^{3+}) \rightarrow ^5\text{F}_5(\text{Ho}^{3+}) + ^2\text{F}_{7/2}(\text{Ce}^{3+})$ (CR1) and $^5\text{I}_6(\text{Ho}^{3+}) + ^2\text{F}_{5/2}(\text{Ce}^{3+}) \rightarrow ^5\text{I}_7(\text{Ho}^{3+}) + ^2\text{F}_{7/2}(\text{Ce}^{3+})$ (CR2). Hence, the introduction of Ce^{3+} ions into $\text{CaF}_2:\text{Yb}^{3+}/\text{Ho}^{3+}$ UCNP s would significantly change the NR probability. These two CR processes result in the population of red emitting level $^5\text{F}_5$ and its intermediate level $^5\text{I}_7$, together with the depopulation of green emitting level $^5\text{S}_2/^5\text{F}_4$ and its intermediate level $^5\text{I}_6$. Thus, the efficient CR processes contribute to the remarkable enhancement of red emission and the suppressed green emission.

Fig. 5(b) displays the dependence of the red and green UC emission as a function of the pump density. Generally, the number of photons required for UC emission is determined by the following formula: $I \propto P^n$, where I represents the UC emission intensity, P is pump power density, and n is the number of photons required for UCL. Thus, the slope of the plot of UC emission intensity as a function of pump density determines

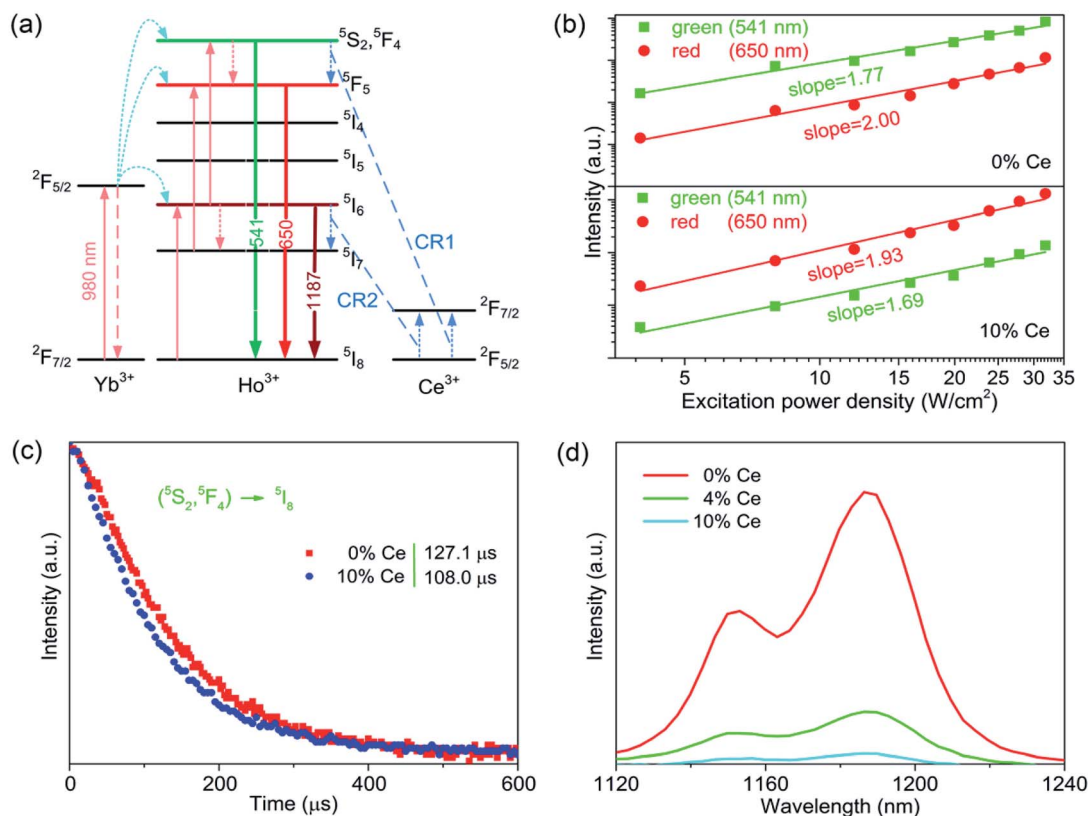


Fig. 5 (a) Schematic energy level diagram and proposed UC mechanism of $\text{CaF}_2:\text{Yb}^{3+}/\text{Ho}^{3+}/\text{Ce}^{3+}$ UCNP s. (b) Pump power dependence of UC emission intensity of Ce^{3+} -free and 10 mol% Ce^{3+} doped $\text{CaF}_2:\text{Yb}^{3+}/\text{Ho}^{3+}$ UCNP s under the excitation of 980 nm CW laser. (c) Decay profiles of $\text{CaF}_2:\text{Yb}^{3+}/\text{Ho}^{3+}$ UCNP s doped with different Ce^{3+} concentrations (0 and 10 mol%) monitored at 541 nm under 980 nm pulse laser excitation. (d) Measured NIR emission spectra of $\text{CaF}_2:\text{Yb}^{3+}/\text{Ho}^{3+}/\text{Ce}^{3+}$ UCNP s with different Ce^{3+} concentrations (0, 4 and 10 mol%) under the excitation of 980 nm CW laser.



the number n in the logarithmic coordinate. In Fig. 5(b), the slopes of green and red UC emissions are all close to 2. It suggests that the red and green UC emissions of these two samples are both two-photon processes. Noted that the number of photons required for green and red emissions of $\text{CaF}_2:\text{Yb}^{3+}/\text{Ho}^{3+}/\text{Ce}^{3+}$ UCNPs is slightly lower than those of $\text{CaF}_2:\text{Yb}^{3+}/\text{Ho}^{3+}$ counterparts. This is attributed to the fact that the population of intermediate level of the red UC emission in $\text{CaF}_2:\text{Yb}^{3+}/\text{Ho}^{3+}$ is cancelled in $\text{CaF}_2:\text{Yb}^{3+}/\text{Ho}^{3+}$ doped with 10 mol% Ce^{3+} ions due to the quenching of the green UC emission.

As illustrated in Fig. 5(c), the decay curves of green UC emission for Ce^{3+} -free and 10 mol% Ce^{3+} doped $\text{CaF}_2:\text{Yb}^{3+}/\text{Ho}^{3+}$ UCNPs are performed under the excitation of 980 nm pulsed laser. The lifetime of the green UC emission was measured to be 127.1 and 108.0 μs for the UCNPs doping with 0 and 10 mol% Ce^{3+} ions, respectively. The decrease of lifetime confirms the existence of the CR1 process. Fig. 5(d) shows the NIR emission (1187 nm, attributed to the transition of $^5\text{I}_6 \rightarrow ^5\text{I}_8$ of Ho^{3+} ions) spectra of $\text{CaF}_2:\text{Yb}^{3+}/\text{Ho}^{3+}$ UCNPs doping with different concentrations of Ce^{3+} ions (0, 4 and 10 mol%). It can be found that the NIR emission intensity decreases as the doped Ce^{3+} ions increase, verifying the occurrence of CR2 process. As discussed above, the addition of Ce^{3+} ions in $\text{Yb}^{3+}/\text{Ho}^{3+}$ codoped materials will lead to the occurrence of CR1 and CR2 processes between the Ce^{3+} and Ho^{3+} ions, resulting in the enhancing red and suppressing green UC emissions.

4. Conclusions

In conclusion, $\text{CaF}_2:\text{Yb}^{3+}/\text{Ho}^{3+}$ (20/2 mol%) UCNPs codoped with different concentrations of Ce^{3+} ions were successfully synthesized by a simple hydrothermal method. Size manipulation was achieved in the $\text{CaF}_2:\text{Yb}^{3+}/\text{Ho}^{3+}$ UCNPs by doping with different concentrations of Ce^{3+} ions. In addition, the introduction of Ce^{3+} ion can greatly suppress the green and enhance the red UC emission, resulting in the luminescence color changing from green to red. The R/G ratios can be varied from 0.17 to 7.44 as the doped Ce^{3+} ions increase from 0 to 10 mol%. The mechanism of the enhancement of red emission has also been demonstrated based on the two CR processes between Ho^{3+} and Ce^{3+} ions, which was supported by the time-resolved decay curves and NIR emissions. The tunability of multicolor and enhancement of red emission make these UCNPs suitable for applications in bioimaging and color display.

Conflicts of interest

There are no conflicts to declare.

Acknowledgements

We would like to gratefully acknowledge the financial support from the State Key Laboratory of Laser Interaction with Matter Foundation (SKLLIM1708).

Notes and references

- 1 Y. Liu, Y. Lu, X. Yang, X. Zheng, S. Wen, F. Wang, X. Vidal, J. Zhao, D. Liu, Z. Zhou, C. Ma, J. Zhou, J. A. Piper, P. Xi and D. Y. Jin, *Nature*, 2017, **543**, 229–233.
- 2 B. Zhou, B. Y. Shi, D. Y. Jin and X. G. Liu, *Nat. Nanotechnol.*, 2015, **10**, 924–936.
- 3 F. Wang, Y. Han, C. S. Lim, Y. H. Lu, J. Wang, J. Xu, H. Y. Chen, C. Zhang, M. H. Hong and X. G. Liu, *Nature*, 2010, **463**, 1061–1065.
- 4 Q. Liu, Y. Sun, T. Yang, W. Feng, C. Li and F. Li, *J. Am. Chem. Soc.*, 2011, **133**, 17122–17125.
- 5 J. Zhou, Z. Liu and F. Li, *Chem. Soc. Rev.*, 2012, **41**, 1323–1349.
- 6 E. M. Dianov, *Light: Sci. Appl.*, 2012, **1**, e12.
- 7 Y. Han, H. Li, Y. Wang, Y. Pan, L. Huang, F. Song and W. Huang, *Sci. Rep.*, 2017, **7**, 1320.
- 8 W. Zou, C. Visser, J. A. Maduro, M. S. Pshenichnikov and J. C. Hummelen, *Nat. Photonics*, 2012, 560–564.
- 9 G. B. Shan and G. P. Demopoulos, *Adv. Mater.*, 2010, **22**, 4373–4377.
- 10 C. Wang, L. Cheng and Z. Liu, *Biomaterials*, 2011, **32**, 1110–1120.
- 11 G. Tian, Z. Gu, L. Zhou, W. Yin, X. Liu, L. Yan, S. Jin, W. Ren, G. Xing, S. Li and Y. Zhao, *Adv. Mater.*, 2012, **24**, 1226–1231.
- 12 J. J. Zhou, J. Y. Deng, H. M. Zhu, X. Y. Chen, Y. Teng, H. Jia, S. Q. Xu and J. R. Qiu, *J. Mater. Chem. C*, 2013, **1**, 8023–8027.
- 13 F. Wang and X. G. Liu, *J. Am. Chem. Soc.*, 2008, **130**, 5642–5643.
- 14 F. Wang and X. G. Liu, *Chem. Soc. Rev.*, 2009, **38**, 976–989.
- 15 Y. Zhang, L. Huang and X. Liu, *Angew. Chem., Int. Ed.*, 2016, **55**, 5718–5722.
- 16 B. Chen, W. Kong, Y. Liu, Y. Lu, M. Li, X. Qiao, X. Fan and F. Wang, *Angew. Chem., Int. Ed.*, 2017, **129**, 10519–10523.
- 17 F. Wang and X. G. Liu, *Acc. Chem. Res.*, 2014, **47**, 1378–1385.
- 18 J. Tang, L. Chen, J. Li, Z. Wang, J. H. Zhang, L. G. Zhang, Y. S. Luo and X. J. Wang, *Nanoscale*, 2015, **7**, 14752–14759.
- 19 J. Wang, F. Wang, C. Wang, Z. Liu and X. Liu, *Angew. Chem., Int. Ed.*, 2011, **50**, 10369–10372.
- 20 W. Gao, R. B. Wang, Q. Y. Han, J. Dong, L. X. Yan and H. R. Zheng, *J. Phys. Chem. C*, 2015, **119**, 2349–2355.
- 21 X. F. Yu, L. D. Chen, M. Li, M. Y. Xie, L. Zhou, Y. Li and Q. Q. Wang, *Adv. Mater.*, 2008, **20**, 4118–4123.
- 22 J. C. Boyer, C. J. Carling, B. D. Gates and N. R. Branda, *J. Am. Chem. Soc.*, 2010, **132**, 15766–15772.
- 23 R. Deng, F. Qin, R. Chen, W. Huang, M. Hong and X. Liu, *Nat. Nanotechnol.*, 2015, **10**, 237–242.
- 24 H. Wen, H. Zhu, X. Chen, T. F. Hung, B. Wang, G. Zhu, S. F. Yu and F. Wang, *Angew. Chem., Int. Ed.*, 2013, **52**, 13419–13423.
- 25 D. D. Li, Q. Y. Shao, Y. Dong, F. Fang and J. Q. Jiang, *Part. Part. Syst. Charact.*, 2015, **32**, 728–733.
- 26 Z. T. Chen, E. H. Song, M. Wu, S. Ding, S. Ye and Q. Y. Zhang, *J. Alloys Compd.*, 2016, **667**, 134–140.
- 27 H. Guo, N. Dong, M. Yin, W. Zhang, L. Lou and S. Xia, *J. Phys. Chem. B*, 2004, **108**, 19205–19209.



- 28 H. Guo and Y. M. Qiao, *Opt. Mater.*, 2009, **31**, 583–589.
- 29 D. Peng, Q. Ju, X. Chen, R. Ma, B. Chen, G. Bai, J. Hao, X. Qiao, X. Fan and F. Wang, *Chem. Mater.*, 2015, **27**, 3115–3120.
- 30 Y. Li, G. F. Wang, K. Pan, N. Y. Fan, S. Liu and L. Feng, *RSC Adv.*, 2013, **3**, 1683–1686.
- 31 K. L. Reddy, V. Srinivas, K. R. Shankar, S. Kumar, V. Sharma, A. Kumar, A. Bahuguna, K. Bhattacharyya and V. Krishnan, *J. Phys. Chem. C*, 2017, **121**, 11783–11793.
- 32 G. Chen, H. Liu, G. Somesfalean, H. Liang and Z. Zhang, *Nanotechnology*, 2009, **20**, 385704.
- 33 T. Pang and J. Wang, *Mater. Res. Express*, 2018, **5**, 015049.
- 34 W. Gao, J. Dong, J. Liu and X. Yan, *Mater. Res. Bull.*, 2016, **80**, 256–262.
- 35 W. Gao, J. Dong, X. Yan, L. Liu, J. Liu and W. Zhang, *J. Lumin.*, 2017, **192**, 513–519.
- 36 T. Li, C. Guo, H. Suo and P. Zhao, *J. Mater. Chem. C*, 2016, **4**, 1964–1971.
- 37 F. Hu, J. Zhang, O. Giraldo, W. Song, R. Wei, M. Yin and H. Guo, *J. Lumin.*, 2018, **201**, 493–499.
- 38 G. Wang, Q. Peng and Y. Li, *J. Am. Chem. Soc.*, 2009, **131**, 14200–14201.
- 39 R. Wang, M. Yuan, C. Zhang, H. Wang and X. Xu, *Opt. Mater.*, 2018, **79**, 403–407.
- 40 X. Deng, Y. Dai, J. Liu, Y. Zhou, P. Ma, Z. Cheng, Y. Chen, K. Deng, X. Li, Z. Hou, C. Li and J. Lin, *Biomaterials*, 2015, **50**, 154–163.
- 41 S. Zeng, Z. Yi, W. Lu, C. Qian, H. Wang, L. Rao, T. Zeng, H. Liu, B. Fei and J. Hao, *Adv. Funct. Mater.*, 2014, **24**, 4051–4059.
- 42 X. Zhao and M. C. Tan, *J. Mater. Chem. C*, 2015, **3**, 10207–10214.

